

EoCD: Encoder only Remote Sensing Change Detection

Mubashir Noman¹ Mustansar Fiaz² Hiyam Debary² Abdul Hannan³ Shah Nawaz⁴
Fahad Shahbaz Khan¹ Salman Khan¹

¹MBZUAI, UAE ²IBM Research, UAE ³University of Trento, Italy
⁴Johannes Kepler University Linz, Austria

Abstract

Being a cornerstone of temporal analysis, change detection has been playing a pivotal role in modern earth observation. Existing change detection methods rely on the Siamese encoder to individually extract temporal features followed by temporal fusion. Subsequently, these methods design sophisticated decoders to improve the change detection performance without taking into consideration the complexity of the model. These aforementioned issues intensify the overall computational cost as well as the network's complexity which is undesirable. Alternatively, few methods utilize the early fusion scheme to combine the temporal images. These methods prevent the extra overhead of Siamese encoder, however, they also rely on sophisticated decoders for better performance. In addition, these methods demonstrate inferior performance as compared to late fusion based methods. To bridge these gaps, we introduce encoder only change detection (EoCD) that is a simple and effective method for the change detection task. The proposed method performs the early fusion of the temporal data and replaces the decoder with a parameter-free multi-scale feature fusion module thereby significantly reducing the overall complexity of the model. EoCD demonstrate the optimal balance between the change detection performance and the prediction speed across a variety of encoder architectures. Additionally, EoCD demonstrate that the performance of the model is predominantly dependent on the encoder network, making the decoder an additional component. Extensive experimentation on four challenging change detection datasets reveals the effectiveness of the proposed method. Code and models are available at <https://github.com/techmn/eocd>.

1. Introduction

Remote sensing acquires a large amount of temporal data, allowing researchers to study and monitor the earth surface over the passage of time. Being a critical task to

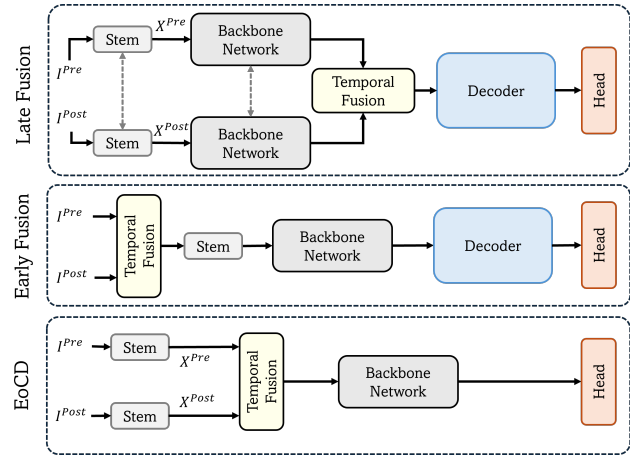


Figure 1. Comparison of various CD frameworks. a) In late fusion, I^{pre} and I^{post} are fed to Siamese encoder causing the backbone network to process each image separately which lead to increased computational cost. b) Early fusion approach prevent this by concatenating the bitemporal images before passing it to backbone, however, the sophisticated decoder still adds undesirable complexity to the model. c) EoCD introduces a simple design that bypasses the extra overhead of Siamese encoder and sophisticated decoder.

investigate changes between temporal data, change detection (CD) has a wide range of applications, including urban planning, deforestation monitoring, disaster analysis, emergency planning, and more. Earlier approaches performed change detection by utilizing change vector analysis [4] and support vector machines [38]. Later, with the rise of deep learning, convolutional neural network (CNN) based approaches have reshaped the problem of CD task. Few methods [9, 21, 36] perform the early fusion of the temporal images and utilize an end-to-end network for change detection. These networks are typically an encoder-decoder segmentation network with the exception that the input is concatenated bitemporal images. The early fusion networks allow for direct interaction of temporal data during feature extraction and provide somehow fair change detection performance, however, these approaches are underexplored by

the remote sensing community.

Alternatively, most of the CNN- and transformer-based CD methods [2, 34, 42, 47] fall into the late fusion category. As illustrated in Fig. 1, a typical CD approach that uses the late fusion scheme is composed of a Siamese encoder (shared stem and backbone), a temporal fusion module, a decoder, and a CD head. The Siamese encoder is responsible for extracting the features from bitemporal images one at a time, and the sophisticated decoder highlights the relevant information necessary for CD task. Both these components usually add computational burden to the overall model’s performance. Although late fusion approaches [26, 35, 54] demonstrate promising CD performance, it is achieved at the expense of a significant increase in computational complexity.

To address the above limitations of late fusion CD models and inspired from the recent work [22], we propose a simple yet efficient CD method that takes the advantages of early fusion and replaces the sophisticated decoder with parameter free multi-scale feature fusion module thereby achieving the optimal CD performance. Unlike traditional early fusion approaches, proposed method projects the bitemporal images to the feature space by using stem layer followed by fusion of bitemporal features as illustrated in Fig. 1. Notably, proposed method does not utilize a decoder enabling it to further reduce the computational cost while maintaining the balance between the performance and efficiency. We summarize our contributions as follows:

- We propose encoder only change detection (EoCD), a simple and efficient change detection model that is based on early fusion strategy and does not utilize the sophisticated CD decoder while achieving promising CD performance.
- We introduce a novel efficient multiscale feature fusion (EMFF) module that does not contain any learnable parameters and emphasize the semantic information in the multiscale representations, thereby providing optimal CD performance.
- We demonstrate that the performance of the change detection models is mainly dependent on the encoder network, making the decoder an additional component and setting a new direction for the remote sensing community.
- Extensive experimentation on four challenging CD datasets with various encoder networks demonstrate the optimal performance revealing the effectiveness of the proposed method.

2. Related Work

2.1. CNN-Based CD Methods

Convolutional neural networks (CNNs) have gained in popularity due to their intrinsic characteristic to extract the powerful feature representation capabilities in computer vi-

sion and remote sensing communities. The advancement of deep learning in remote sensing change detection (RSCD) tasks can be roughly categorized as early fusion and late fusion. The early fusion approaches first combine the bitemporal input images and process them through a single encoder-decoder segmentation network [1, 10, 36]. Alcantarilla et al. [1] first concatenate the two images into six-channel input and pass it to FCN to realize the street view CD. Fang et al. [13] propose, named SNUNet-CD, a densely connected Siamese network for comprehensive interaction between the input bitemporal images for change detection. Peng et al. [36] used UNet++ model with dense skip connections to learn multiscale and various levels of feature representations. Jiang et al. [21] propose a weighted scale block, which dynamically assigns appropriate weights to multiscale features to obtain accurate detection.

Late fusion approaches utilize a shared backbone to extract high-level features for the bitemporal input features and fuse them by employing different operations such as subtraction, multiplication, or concatenation for the change detection task [8, 9]. Daudt et al. [9] propose FC-Siam-Conv, which utilizes a Siamese CNN to fuse bi-temporal images along the channel dimension and process them for the CD task. Zhang et al. [53] used transfer learning to form a two-channel network with shared weights to extract multiscale and multi-depth features using a change magnitude guided loss function. DTCDSN [30], SNUNet-CD [13], and IFN [47] exploit channel and spatial attention mechanisms to learn the spatially robust features. These approaches aim to extract both low-level features to assist in target localization as well as high-level features to enrich the semantic information for better change detection. Zhang et al. [49] introduced the superpixel enhanced CD network (ESCNet), which takes advantage of superpixel segmentation to reduce latent noise in pixel-level feature maps while preserving edges, and two weight-sharing superpixel sampling networks (SSNs) tailored for feature extraction. Lv et al. [32] proposed to integrate an adaptively generated change magnitude image (CMI), which guides the CD model to capture the shape and sizes of the changing regions. Huang et al. [19] proposed a spatiotemporal difference enhancement and adaptive context fusion to aggregate feature maps from multiple scales. Huang et al. [18] introduce the MASNet CD method based on selective fusion of multi-temporal features by constructing selective convolutional kernels and multiple attention modules. Lei et al. [24, 27] proposed a lightweight CD networks that utilize an attention operation to recalibrate the feature channels for feature enhancement. Han et al. [16] introduced a lightweight model by artificial padding convolution and design a new loss function for the bitemporal CD task. Despite the effectiveness of the aforementioned approaches, the CNN-based methods face challenges in capturing the

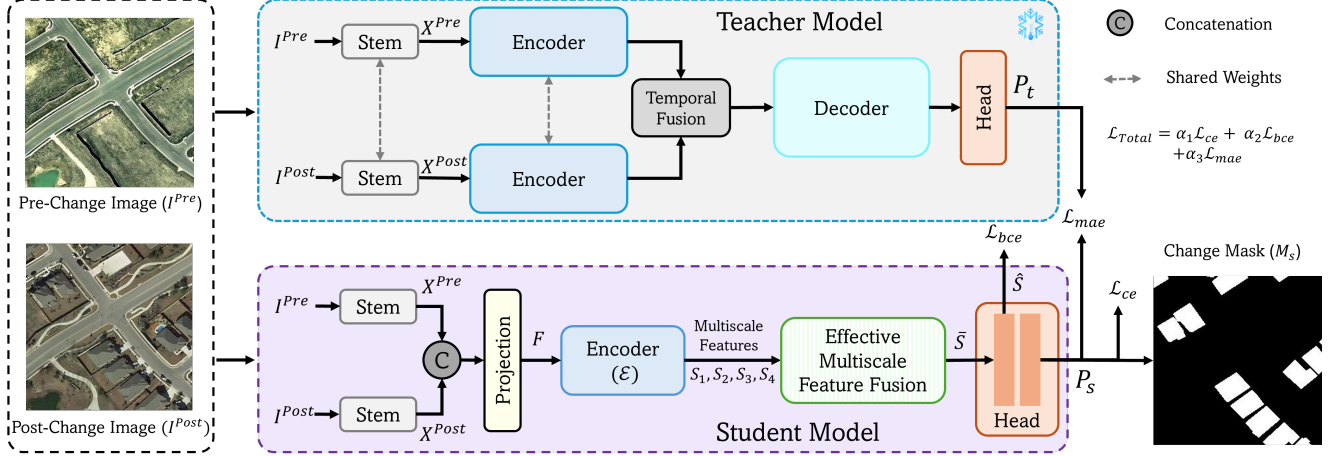


Figure 2. Overall architecture of the proposed EoCD. It characterizes a student-teacher framework with a decoder-less student network. The student network performs early fusion of temporal images and optimally combines the multiscale representations, thereby significantly improving the efficiency of the network.

long-range dependencies due to their inherent local receptive field attributes, which limit the ability to extract global relationships for better prediction of multiscale regions.

2.2. Transformer-based CD Methods

With the recent success of transformers [12] and due to their powerful global context modeling in computer vision, it has drawn attention in the field of CD. Chen et al. [6] proposed a bi-temporal image transformer (BIT), which utilizes the ResNet18 [17] to extract features, followed by a transformer encoder to capture global contextual relationships for the change detection. Bandara et al. [2] introduced ChangeFormer, which leverages the vision Transformer as a backbone for extracting bi-temporal image features. Noman et al. [35] proposed ScratchFormer, which is trained from scratch and employs a shuffled sparse-attention operation, and aims to select sparse informative regions to capture the inherent characteristics of the CD data. Zhang et al. [48] employed SwinTransformer [31] to extract multi-scale features. Liu et al. [28] utilized deep supervision to exploit the multi-scale features and performed multi-scale supervision. ELGCNet [34] employed a Siamese network that encodes global context and local spatial information through a pooled-transpose (PT) attention and depthwise convolution. Li et al. [26] proposed TransUNetCD, which integrates UNet and Transformer within an encoder-decoder framework. Zhang et al. [50] introduced a CD method called BIFA, which incorporates spatial-temporal alignment and multiscale alignment. Zhang et al. [52] proposed spatial-temporal robust representation learning by enhancing model efficiency and reducing inconsistent bitemporal features confusion. Although these transformer-based methods have achieved great performance, they exhibit quadratic

complexity with respect to tokens, which leads to significant computational costs and limits their practicality for dense prediction tasks such as CD.

Recently, Mamba [15] has shown great success in the CV field [43, 46, 55] and received much attention due to inherent characteristics such as time-varying parameters into State Space Models (SSMs), enabling data-dependent global modeling with linear complexity. Zhao et al. [54] proposed RSMamba, which utilizes a selective scan module to encode the global context information in multiple directions, capturing large spatial features from various directions. Chen et al. [7] introduced ChangeMamba, a Mamba-based architecture, to fully learn spatio-temporal features. CDMamba [51] leverages from state space models and CNNs to dynamically combine global and local features for the CD task.

All of these aforementioned approaches utilize Siamese encoder network, temporal fusion, a decoder, and a CD head. Although a shared Siamese network extracts meaningful features, it increases the computational complexity. Furthermore, a dedicated decoder is effective for improving CD performance, however, it results in an undesired increase in computational requirements and model parameters. In contrast, we intend to propose a simple but elegant framework that mitigates the requirement of a Siamese encoder and a decoder, while discriminating the complex change regions with better accuracy.

3. Method

3.1. Preliminaries

We denote the bitemporal images acquired at different time intervals as $I^{pre} \in \mathbb{R}^{3 \times H \times W}$ and $I^{post} \in \mathbb{R}^{3 \times H \times W}$, where

I^{pre} is acquired earlier than I^{post} . Given a pair of bitemporal images $p = (I^{pre}, I^{post})$, the objective of change detection is to highlight the semantic changes between the image pair and predict a binary mask $\mathcal{M} \in \mathbb{R}^{H \times W}$.

Baseline Framework: Considering the efficiency of the model is vital, we adopt the early fusion approach as a baseline framework. The baseline framework takes a bitemporal image pair (I^{pre}, I^{post}) and passes it to separate stem layers extracting the feature representations X^{pre} and X^{post} . These feature representations are concatenated, fed to convolution layers, and passed to an encoder \mathcal{E} . The obtained multiscale feature maps from the encoder are interpolated, then concatenated along the channel dimension, and passed to a convolution layer followed by input to the segmentation head to predict the change map.

The early fusion in the baseline framework significantly reduces the computations since it eliminates a full encoder pass; however, it also considerably degrades the performance of the model which is undesirable. Additionally, naive replacement of the decoder with a convolution layers further limits the ability of the model to perform favorably for change detection task. To this end, we designed an encoder only change detection network that replaces the decoder with an effective multi-scale feature fusion module having no learnable parameters while exploiting the benefits of early fusion for promising change detection performance. We describe this approach in detail as follows.

3.2. EoCD Framework

As illustrated in Fig. 2, the proposed encoder only change detection (EoCD) is a distillation-based teacher-student framework. The teacher network is composed of a Siamese encoder, a bitemporal and multi-scale feature fusion module comprising of layers having learnable parameters, a decoder, and a CD head. Despite the fact that the student network utilizes early fusion of temporal features, its effective design enables it to perform favorably on the change detection task. The student network consists of an encoder, an effective multi-scale feature fusion (EMFF) module having no learnable parameters, and a CD head. Unlike typical change detection approaches, the proposed EoCD approach instills semantic information from the teacher CD network to the decoder-less student network for explicit enhancement of student representations.

3.2.1. Student Network Architecture

Given a bitemporal image pair $p = (I^{pre}, I^{post})$, we pass I^{pre} to the stem layer to obtain features X^{pre} . Similarly, we feed I^{post} to the stem layer to obtain features X^{post} . Afterwards, we concatenate the features X^{pre} and X^{post} followed by input to the convolution layers obtaining the fused temporal representations F . Mathematically, these operations are represented as:

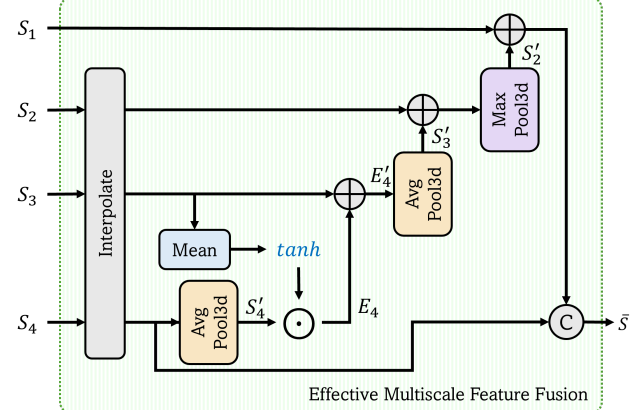


Figure 3. Architecture of efficient multiscale feature fusion (EMFF) module. EMFF effectively combines the multiscale features while reducing the computational cost.

$$\begin{aligned} X^{pre} &= \text{Conv}_{pre}(I^{pre}), \quad X^{post} = \text{Conv}_{post}(I^{post}) \\ X &= \text{Concat}(X^{pre}, X^{post}) \\ F &= \text{DWConv}(\text{Conv}(\text{DWConv}(X))) \end{aligned} \quad (1)$$

Consequently, we input the feature representations F into the encoder \mathcal{E} to obtain the multi-scale features S_j where $j \in [1, 2, 3, 4]$ represents the j th stage of the encoder. These multiscale features S_j are effectively fused by the EMFF module to obtain semantically enhanced features \bar{S} . Finally, the fused representations are passed to the change detection head that provides the change probabilities P_s to obtain the binary change mask \mathcal{M}_s .

3.2.2. Effective Multiscale Feature Fusion Module

As discussed in Sec. 3.1 that the naive fusion of multiscale features increases the computational complexity of the network while struggling to provide favorable CD performance, therefore, an effective strategy was required for optimal fusion of multiscale representations. We designed the effective multiscale feature fusion (EMFF) module to achieve this objective, as illustrated in Fig. 3. Notably, proposed EMFF module does not utilize any learnable parameters layer while being capable of highlighting the critical information within the multiscale representations. The proposed EMFF module takes the multiscale features S_j and interpolates them to obtain the features having same spatial resolution. Afterwards, it first applies average pooling operation on the features S_4 along the channel dimension to obtain the average response S'_4 within a local neighborhood while making its channel dimension same as the features S_3 . To focus on semantically relevant information, we take the mean of features S_3 along channel dimension, apply the $tanh$ activation and multiply it with the pooled features S'_4 to get enhanced features E_4 . Later we add the representations E_4 and S_3 . Mathematically, these operations are as follows:

Table 1. Summary of remote sensing change detection (RSCD) datasets and their attributes i.e., number of image pairs, image sizes, spatial resolution, splits, image types and change types.

Dataset	Image Pairs	Image Size	Spatial Resolution	Train/Val/Test	Image Type	Change Type
LEVIR-CD [5]	637	1024 × 1024	0.5 m/pixel	7120 / 1024 / 2048	satellite images	building
CDD-CD [23]	11	4725 × 2700 & 1900 × 1000	0.03–1 m/pixel	10000 / 3000 / 3000	satellite images	building, road
SYSU-CD [37]	20000	256 × 256	0.5 m/pixel	12000 / 4000 / 4000	aerial images	building, vegetation, road
WHU-CD [20]	1	32207 × 15354	0.075 m/pixel	5947 / 743 / 744	aerial images	building

$$\begin{aligned}
 w &= \tanh(\text{mean}_c(S_3)) \\
 S'_4 &= \text{AvgPool}_c(S_4) \\
 E_4 &= w \odot S'_4 \\
 E'_4 &= S_3 + E_4
 \end{aligned} \tag{2}$$

After obtaining the enhanced representations E'_4 , we further pass it to the average pooling layer to decrease the channel dimension and obtain the features S'_3 that depict the mean response within a local neighborhood. These features are then added to the representations S_2 and fed to the max pooling layer highlighting the significant information and obtaining the features S'_2 . Finally, we add the feature representations S_1 and S'_2 to focus on the fine grained information, followed by concatenation with the features S_4 to obtain semantically rich representations (\bar{S}).

3.2.3. Training Phase

During the training phase, the bitemporal images are first passed to the teacher network and obtain the teacher predictions P_t . The teacher network is kept frozen during training. Subsequently, input images are passed to the student network and obtain the student predictions P_s along with the intermediate output representations \hat{S} as illustrated in Fig. 2.

We optimize the entire EoCD framework in an end-to-end fashion using a combination of losses. *Cross-Entropy* loss \mathcal{L}_{ce} is utilized on the student predictions P_s , encouraging it to align the predictions with the ground-truth change mask. To further boost the student network's ability to accurately distinguish between the changed and unchanged pixels, we utilize the *Binary Cross-Entropy* loss \mathcal{L}_{bce} on the intermediate output \hat{S} . Finally, we enable the network to improve its performance by instilling the information contained in the teacher's predictions P_t and utilize the mean absolute error loss \mathcal{L}_{mae} between the teacher and student predictions. The final training objective becomes the combination of three losses as follows:

$$\mathcal{L}_{Total} = \alpha_1 \mathcal{L}_{ce} + \alpha_2 \mathcal{L}_{bce} + \alpha_3 \mathcal{L}_{mae} \tag{3}$$

4. Experiments

4.1. Implementation Details

Our EoCD method is implemented in PyTorch using single A100 GPU, which takes a pair of images of size 256×256 . During training, the pair of images is passed to both teacher

and student models. In the training pipeline, we incorporate random flop, color jitter, scale-crop, and Gaussian blur augmentation techniques to enhance the generalization capabilities. We set our teacher network as HyRet-Change [14] since it provides promising results on CD task, however, any large network either based on late or early fusion can be utilized as a teacher network. The student network utilized in experiments is FocalNet-T [45] unless otherwise specified in the paper. Following [2, 6, 34], we set batch size to 32, learning rate to $3e-4$ and trained for 600 epoch. We used AdamW optimizer and set weight decay to 0.01, beta values equal to (0.9, 0.999), and used linear decay to decrease the learning rate to 0 until the last epoch.

4.2. Datasets

We perform extensive experiments over four publicly available datasets as illustrated in table 1.

LEVIR-CD [5] It is a large-scale bi-temporal remote sensing change detection benchmark dataset which consists of 637 pairs of images. Each image size is 1024×1024 with 0.5m per pixel spatial resolution. This dataset covers building related changes such as apartments, housing structures, warehouse, and compact garages, over a 5 to 14-year span in multiple cities across Texas, USA. The images are captured from Google Earth and follow the partitioning protocol (7:1:2). The original images are cropped into non-overlapping patches of 256×256 , yielding 7120 train samples, 1024 validation samples, and 2048 test samples.

CDD-CD [23] This challenging CD benchmark dataset consists of 11 pair of raw images captured from Google Earth, with seven image pairs of size 4725×2700 pixels and four image pairs of size 1900×1000 , from 0.03m to 1m per pixel. This is a challenging dataset due to complex scenarios including seasonal variations, man-made infrastructures (buildings and road infrastructure) and natural features (vegetation/forest cover). This dataset is available in uniformly cropped images of size 256×256 which results in 16000 image pairs. These cropped images are available in split of 10,000, 3000, and 3000 for the training, validation, and test purposes, respectively.

SYSU-CD [37] This dataset comprises of 20,000 ultrahigh resolution images of size 256×256 and the ground sample distance resolution of 0.5m, acquired between 2007 and 2014 in Hong Kong region. This dataset pose various land-cover change types, including vegetation changes, road/transportation expansions, newly constructed urban

Table 2. Performance comparison of the state-of-the-art methods on LEVIR-CD. FLOPs and Latency are computed using RGB image size of 224×224 . Our approach achieves superior performance in terms of IoU, F1, and overall accuracy metrics and shows favorable performance against existing approaches. Best results are highlighted in darker color.

Method	Backbone	Params (M)	FLOPs (G)	Latency (msec)	IoU (%)	F1 (%)	Accuracy (%)
EATDer [33]	Custom	7.12	21.30	26.2	-	91.20	98.75
ELGCNet-LW [34]	Custom	6.78	15.17	24.5	82.36	90.33	99.03
ChangeFormer [2]	Custom	41.03	106	26.6	82.48	90.40	99.04
Convformer-CD/48 [44]	Custom	49.31	5.3	48.8	84.23	91.44	99.13
RSMamba [†] [54]	Mamba	27.90	15.70	-	83.66	91.10	-
CDMamba [†] [51]	Mamba	11.91	49.26	54.77	83.07	90.75	99.06
BIT [6]	ResNet-18	12.40	8.32	13.3	80.68	89.31	98.92
STRobustNet [52]	ResNet-18	13.73	19.32	12.7	83.66	91.11	99.10
TMSF [40]	ResNet-18	12.92	8.90	40.4	83.29	90.88	-
FSG-Net [42]	ResNet-18	13.76	-	-	83.94	91.27	99.10
RHighNet [†] [11]	Resnet50 + ViT-B/16	120.8	69.47	98.9	84.01	91.31	99.13
SFEARNet [25]	SegFormer [41]	5.56	3.64	26.7	83.23	90.85	99.07
DSFDcd [39]	U-Net	8.94	-	-	80.34	89.11	98.93
EoCD (Ours)	mit-b1	13.37	2.49	8.1	83.20	90.83	99.08
EoCD (Ours)	ResNet-34	21.50	4.39	3.8	83.33	90.91	99.09
EoCD (Ours)	FocalNet-T	30.32	6.46	12.1	84.78	91.76	99.17

[†] denotes that the FLOPs and Latency is reported using image size of 256×256 due to issues with model configuration

buildings, sea construction, and pre-construction ground works. For experimental comparison, we utilize standard split provided, which has 12,000 pairs of images for training and 4000 pairs for validation and testing, corresponding to a ratio of 6:2:2.

WHU-CD [20] WHU building dataset is another aerial building-related CD benchmark dataset which consists of 1 high-resolution (0.075m) image pair of size 32207×15354 pixels. This dataset is challenging due to the variety of building infrastructures, such as countryside, residential, and industrial areas, with different sizes and colors. The data set is cropped into non-overlapping regions of size 256×256 , and is divided into 5947, 743, and 744 image pairs for the training, validation, and test sets, respectively.

4.3. Evaluation Protocol

Following prior works [2, 6, 34, 52], we utilize the change-class intersection over union (IoU), F1 score, and overall accuracy to measure the performance of the model. In addition, we utilize learnable parameters, floating-point operations per second (FLOPs) and latency to evaluate the computational complexity of the model. For fair comparison, we utilize the publicly available official repositories of the compared methods to verify the number of parameters and FLOPs. Additionally, we use the Quadro RTX 6000 GPU to compute the latency of all methods.

4.4. Quantitative Comparison

Here, we discuss the quantitative comparison of our approach with other state-of-the-art (SOTA) methods over LEVIR-CD, CDD-CD, SYSU-CD, and WHU-CD benchmark datasets.

LEVIR-CD: We compare the performance of the proposed EoCD with SOTA methods on the LEVIR-CD dataset in Tab. 2. We observe that recent Convformer-CD/48 [44] provides promising results by achieving the IoU score of 84.23% and FLOPs of 5.3G while having high latency and large number of parameters i.e., 48.8 msec and 49.31M respectively. Similarly, RHighNet [11] is another SOTA method having 69.47 GFLOPs and 120.8M parameters while achieving IoU score of 84.01%. Although SFEARNet [25], utilizing light-weight backbone [41], provides fewer parameters and FLOPs, it has high latency of 26.7 msec while it obtains an IoU of 83.23%. Other notable methods include RSMamba [54], STRobustNet [52], and TMSF [40] obtaining the IoU scores of 83.66%, 83.66%, and 83.29%, respectively, while possessing a greater number of GFLOPs. In contrast, our method obtains state-of-the-art IoU score of 84.78% while exhibiting lower latency and FLOPs, which demonstrates the merits of our approach. Notably, EoCD provides a balance between computational complexity and CD performance by utilizing the small sized encoder. These results demonstrate the adaptability of our encoder only CD approach, highlighting its effectiveness without utilizing a sophisticated decoder.

CDD-CD: In Table 3, we compare our approach with existing SOTA methods over CDD-CD. It is noticeable that TMSF [40], ELGCNet-LW [34], and RHighNet [11] attain IoU score of 90.44%, 93.48%, and 94.65%. Whereas all other approaches exhibit IoU score less than 90%. On this challenging dataset, our approach surpasses other methods and shows consistent performance over IoU, F1, and OA metrics obtaining scores of 94.83%, 97.34%, and 99.37%,

Table 3. SOTA comparison on CDD-CD dataset. We notice that our approach achieves superior performance in terms all metrics and shows favorable performance against existing approaches. Best results are highlighted in darker color.

Method	IoU (%)	F1 (%)	Accuracy (%)
BIT [6]	80.01	88.90	97.47
ChangeFormer [2]	81.53	89.83	97.68
ChangeMamba [7]	81.99	90.10	97.72
STRobustNet [52]	88.08	93.66	98.50
ConvFormer-CD [44]	88.63	93.96	98.59
CDMamba [51]	88.81	94.06	98.57
DSFDcd [39]	88.81	94.06	98.57
FSG-Net [42]	88.96	94.16	98.56
TMSPF [40]	90.44	94.98	-
EATDer [33]	-	95.97	98.97
ELGCNet-LW [34]	93.48	96.63	99.21
RHighNet [11]	94.65	97.25	99.35
EoCD (Ours)	94.83	97.34	99.37

Table 4. SOTA comparison on SYSU-CD benchmark dataset. Our approach performs significantly better compared to existing CD-methods. Best results are highlighted in darker color.

Method	IoU (%)	F1 (%)	Accuracy (%)
ChangeFormer [2]	60.60	75.46	89.20
BIT [6]	61.40	76.08	88.95
ELGCNet [34]	66.62	79.97	90.72
STRobustNet [52]	67.59	80.66	91.13
ConvFormer-CD/48 [44]	65.76	79.35	90.98
ChangeMamba [7]	66.39	79.80	90.85
LCD-Net [29]	68.38	81.22	-
DSFDcd [39]	67.31	80.46	91.00
RHighNet [11]	67.53	80.62	91.33
EoCD (Ours)	68.67	81.42	91.67

respectively.

SYSU-CD: We also evaluate our approach over SYSU-CD benchmark dataset in table 4. We observe that BIT [6] and ChangeFormer [2] struggle on this data set and achieve an IoU of 61.40% and 60.60%. Our approach attains a gain of 7.27% and 8.07% over these well known CD methods. However, compared to recent models including LCD-Net [29], STRobustNet [52], RHighNet [11], and DSFDcd [39], our method shows consistent improvement in terms of IoU, F1, and overall accuracy metrics and demonstrates favorable performance.

WHU-CD: Table 5 further illustrates the performance comparison of our approach with existing SOTA methods over WHU-CD dataset. We notice that BIT [6] and ChangeFormer [2] struggle a lot on this dataset. Recent prominent methods such as STRobustNet [52] and RHighNet [11] obtain IoU score of 83.29% and 83.79%, whereas our approach demonstrates a significant gain of 3.88% and 3.38%, respectively. In addition, ConvFormer-CD [44] and SFEARNet [25] perform better and present IoU score of 85.41% and 85.81%. Our method obtains 87.17% IoU surpassing these methods and attains an absolute gain of 1.76% and 1.36%, respectively. These results demonstrate the elegance of encoder only CD framework by achieving a consistent improvement across all metrics.

Table 5. SOTA comparison on WHU-CD benchmark dataset. Our approach exhibits substantial progress across the metrics compared to existing CD-methods and shows consistent performance gain, indicating better capabilities of our approach to capture the semantic changes. Best results are highlighted in darker color.

Method	IoU (%)	F1 (%)	Accuracy (%)
BIT [6]	72.39	83.98	98.75
ChangeFormer [2]	73.80	84.93	98.82
ELGCNet [34]	80.86	89.42	99.20
ScratchFormer [35]	84.97	91.89	99.37
EATDer [33]	-	90.01	98.58
STRobustNet [52]	83.29	90.89	99.32
ConvFormer-CD [44]	85.41	92.13	99.26
RSMamba [54]	84.96	91.87	-
TMSPF [40]	80.09	88.95	-
RHighNet [11]	83.79	91.18	99.32
SFEARNet [25]	85.81	92.36	99.38
EoCD (Ours)	87.17	93.15	99.47

Table 6. Ablation study demonstrating the effectiveness of the proposed components on LEVIR-CD utilizing FocalNet-T [45] backbone.

Method	Params (M)	FLOPs (G)	IoU (%)	F1 (%)	Accuracy (%)
Baseline	31.23	9.30	80.83	89.40	98.97
Baseline + EMFF	30.32	6.46	82.08	90.15	99.05
Baseline + EMFF + \mathcal{L}_{bce}	30.32	6.46	82.77	90.57	99.89
Baseline + EMFF + \mathcal{L}_{bce} + \mathcal{L}_{mae}	30.32	6.46	84.78	91.76	99.17

4.5. Qualitative Comparison

In figure 4, we present a qualitative comparison of our approach with existing BIT [6], ELGC-Net [34], and ChangeFormer [2]. We notice that EoCD is capable of capturing semantic changes at multiple scales under complex scenarios. For instance, in first and second rows corresponding to LEVIR-CD and CDD-CD respectively, our method detects the semantic change regions fairly better compared to other methods. Furthermore, illustrated images in third and fourth rows which correspond to SYSU-CD and WHU-CD, our method performs favorably and captures the change region boundaries better whereas existing methods struggle on these complex scenes. These results demonstrate the strong capability of EoCD by accurately detecting the relevant semantic changes.

4.6. Ablation Experiments

EoCD Components: Tab. 6 presents the effectiveness of proposed components of EoCD. We observe that the baseline network provides unsatisfactory performance by achieving IoU score of 80.83% while suffering from greater number of FLOPs. When EMFF replaces the convolution-based multiscale feature fusion in baseline network, CD performance is improved by achieving better IoU score of 82.08% while parameters and GFLOPs are reduced to 30.32 and 6.46, respectively. The performance of the network is further improved when we utilize \mathcal{L}_{bce} on the intermediate output features \bar{S} . Finally, the proposed EoCD (row 4

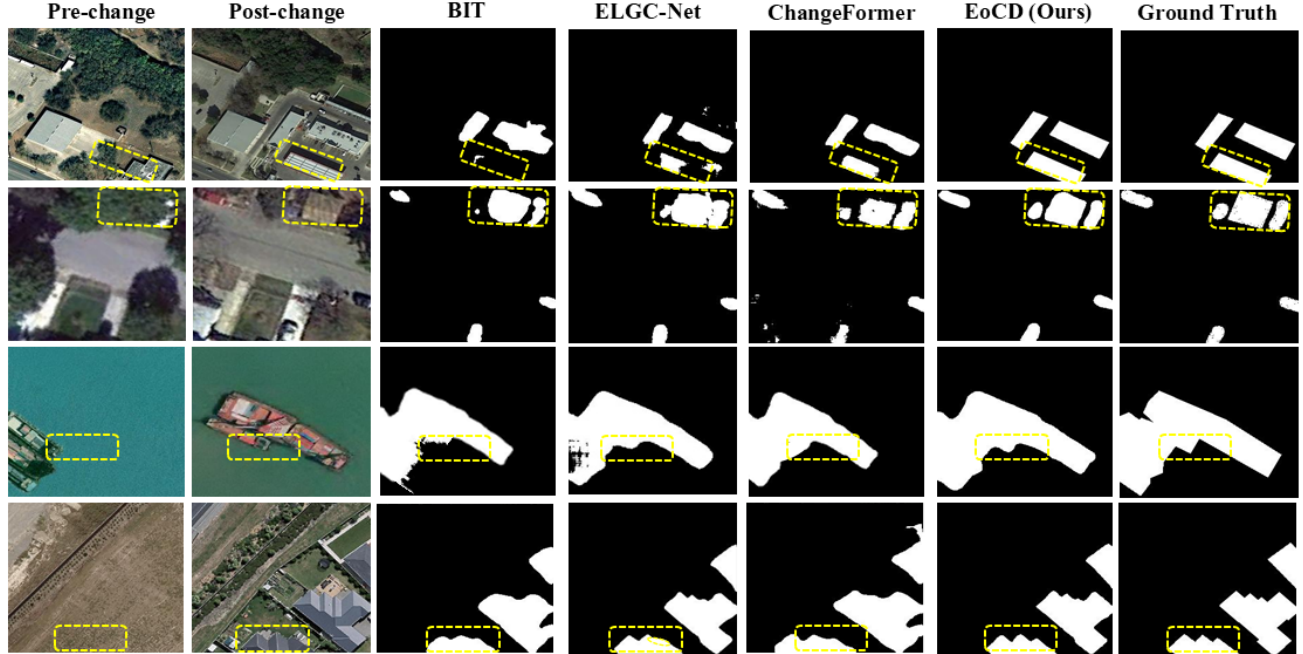


Figure 4. Qualitative comparison of EoCD with BIT [6], ChangeFormer [2], and ELGC-Net [34] CD methods. Data samples shown from row one to four correspond to LEVIR-CD, CDD-CD, SYSU-CD, and WHU-CD datasets, respectively. Notably, our approach demonstrates its capabilities to better detect the semantic changes highlighted in the yellow dotted boxes compared to existing methods.

Table 7. Demonstration of various losses utilized for information distillation on LEVIR-CD utilizing FocalNet-T [45] backbone.

Method	\parallel	$Loss(P_s)$	$Loss(P_s, P_t)$	IoU (%)	F1 (%)	Accuracy (%)
EoCD	CE	KL Div	82.53	90.43	99.05	
	CE	MSE	83.84	91.21	99.11	
	mIoU	MAE	84.56	91.63	99.15	
	CE	MAE	84.78	91.76	99.17	

in Tab. 6) framework provides significant performance improvement obtaining IoU score of 84.78%.

Ablation of Losses: In Tab. 7, we demonstrate the impact of different losses on the performance of the proposed EoCD. From the table, we observe that the Cross Entropy (CE) loss (\mathcal{L}_{ce} in Fig. 2) when combined with mean absolute error (MAE) loss provides the best IoU score of 84.78%. The replacement of CE loss with mIoU loss slightly degrades the performance to 84.56%. Whereas using KL divergence loss or mean squared error loss in place of MAE loss results in noticeable performance reduction as illustrated in first two rows of the table.

How various encoders affect the performance: We further investigate the effect of different encoder architectures on the performance of the EoCD. From Tab. 8, we notice that the CNN based encoder such as ResNet-34 provides optimal tradeoff between CD performance and speed by achieving IoU score of 83.33% and latency of 3.8 msec. Whereas the utilization of transformer-based backbone such as mit-b0 [41] provides acceptable results by achieving

Table 8. Performance comparison of various backbone networks utilized in the EoCD framework on LEVIR-CD.

Backbone	\parallel	Params (M)	FLOPs (G)	Latency (msec)	IoU (%)	F1 (%)	Accuracy (%)
mit-b0 [41]		3.37	0.69	7.9	81.23	89.45	98.96
mit-b1 [41]		13.37	2.49	8.1	83.20	90.83	99.08
ResNet-34 [17]		21.50	4.39	3.8	83.33	90.91	99.09
DebiFormer-T [3]		21.19	3.79	31.2	83.63	91.09	99.11
FocalNet-T [45]		30.32	6.46	12.1	84.78	91.76	99.17

IoU score of 81.23% while its latency is increased to 7.9 msec despite of having less number of FLOPs as compared to ResNet-34. We observe similar trend between the FocalNet-T and DebiFormer-T encoders. From these results, we infer that the CNN based encoder maintain better balance between the CD performance and latency despite of having greater number of parameters and FLOPs compared to transformer based encoders.

5. Conclusion

This work introduces a simple yet effective framework, named as EoCD, for change detection task. The proposed framework is based on early fusion of temporal features and replaces the decoder with a parameter-free feature fusion module (EMFF) demonstrating that early fusion networks are capable of achieving favorable performance while considerably reducing the computational overhead. Proposed EoCD further reveals that the performance of change detection is primarily dependent on the encoder network. Furthermore, we conclude that parameter-free feature fusion is

capable of emphasizing the significant information necessary for change detection while maintaining a balance between optimal performance and efficiency.

References

- [1] Pablo F Alcantarilla, Simon Stent, German Ros, Roberto Arroyo, and Riccardo Gherardi. Street-view change detection with deconvolutional networks. *Autonomous Robots*, 42(7):1301–1322, 2018. [2](#)
- [2] Wele Gedara Chaminda Bandara and Vishal M Patel. A transformer-based siamese network for change detection. In *IGARSS 2022-2022 IEEE International Geoscience and Remote Sensing Symposium*, pages 207–210. IEEE, 2022. [2, 3, 5, 6, 7, 8](#)
- [3] NguyenHuu BaoLong, Chenyu Zhang, Yuzhi Shi, Tsubasa Hirakawa, Takayoshi Yamashita, Tohgoroh Matsui, and Hiironobu Fujiyoshi. Debiformer: Vision transformer with deformable agent bi-level routing attention. In *Proceedings of the Asian Conference on Computer Vision*, pages 4455–4472, 2024. [8](#)
- [4] Francesca Bovolo, Silvia Marchesi, and Lorenzo Bruzzone. A framework for automatic and unsupervised detection of multiple changes in multitemporal images. *IEEE Transactions on Geoscience and Remote Sensing*, 50(6):2196–2212, 2012. [1](#)
- [5] Hao Chen and Zhenwei Shi. A spatial-temporal attention-based method and a new dataset for remote sensing image change detection. *Remote sensing*, 12(10):1662, 2020. [5](#)
- [6] Hao Chen, Zipeng Qi, and Zhenwei Shi. Remote sensing image change detection with transformers. *IEEE Transactions on Geoscience and Remote Sensing*, 60:1–14, 2022. [3, 5, 6, 7, 8](#)
- [7] Hongruixuan Chen, Jian Song, Chengxi Han, Junshi Xia, and Naoto Yokoya. Changemamba: Remote sensing change detection with spatiotemporal state space model. *IEEE Transactions on Geoscience and Remote Sensing*, 62:1–20, 2024. [3, 7](#)
- [8] Jie Chen, Ziyang Yuan, Jian Peng, Li Chen, Haozhe Huang, Jiawei Zhu, Yu Liu, and Haifeng Li. Dasnet: Dual attentive fully convolutional siamese networks for change detection in high-resolution satellite images. *IEEE Journal of Selected Topics in Applied Earth Observations and Remote Sensing*, 14:1194–1206, 2020. [2](#)
- [9] Rodrigo Caye Daudt, Bertr Le Saux, and Alexandre Boulch. Fully convolutional siamese networks for change detection. In *2018 25th IEEE international conference on image processing (ICIP)*, pages 4063–4067. IEEE, 2018. [1, 2](#)
- [10] Pablo Pozzobon De Bem, Osmar Abílio de Carvalho Júnior, Renato Fontes Guimarães, and Roberto Arnaldo Trancoso Gomes. Change detection of deforestation in the brazilian amazon using landsat data and convolutional neural networks. *Remote Sensing*, 12(6):901, 2020. [2](#)
- [11] Huihui Dong, Xinyu Du, Zhijie Li, Zongfang Ma, Yumeng Wang, Hao Zhu, and Wenping Ma. Relation-aware high-order interaction network for remote sensing image change detection. *IEEE Transactions on Geoscience and Remote Sensing*, 2025. [6, 7](#)
- [12] Alexey Dosovitskiy. An image is worth 16x16 words: Transformers for image recognition at scale. *arXiv preprint arXiv:2010.11929*, 2020. [3](#)
- [13] Sheng Fang, Kaiyu Li, Jinyuan Shao, and Zhe Li. Snunet-cd: A densely connected siamese network for change detection of vhr images. *IEEE Geoscience and Remote Sensing Letters*, 19:1–5, 2021. [2](#)
- [14] Mustansar Fiaz, Mubashir Noman, Hiyam Debary, Kamran Ali, and Hisham Cholakkal. Hyret-change: A hybrid repetitive network for remote sensing change detection. *arXiv preprint arXiv:2506.12836*, 2025. [5](#)
- [15] Albert Gu and Tri Dao. Mamba: Linear-time sequence modeling with selective state spaces. In *First conference on language modeling*, 2024. [3](#)
- [16] Min Han, Ran Li, and Chengkun Zhang. Lwcdnet: A lightweight fully convolution network for change detection in optical remote sensing imagery. *IEEE Geoscience and Remote Sensing Letters*, 19:1–5, 2022. [2](#)
- [17] Kaiming He, Xiangyu Zhang, Shaoqing Ren, and Jian Sun. Deep residual learning for image recognition. In *Proceedings of the IEEE conference on computer vision and pattern recognition*, pages 770–778, 2016. [3, 8](#)
- [18] Jiru Huang, Qian Shen, Min Wang, and Mengyuan Yang. Multiple attention siamese network for high-resolution image change detection. *IEEE Transactions on Geoscience and Remote Sensing*, 60:1–16, 2021. [2](#)
- [19] Yanyuan Huang, Xinghua Li, Zhengshun Du, and Huanfeng Shen. Spatiotemporal enhancement and interlevel fusion network for remote sensing images change detection. *IEEE Transactions on Geoscience and Remote Sensing*, 62:1–14, 2024. [2](#)
- [20] Shunping Ji, Shiqing Wei, and Meng Lu. Fully convolutional networks for multisource building extraction from an open aerial and satellite imagery data set. *IEEE Transactions on geoscience and remote sensing*, 57(1):574–586, 2018. [5, 6](#)
- [21] Yu Jiang, Lei Hu, Yongmei Zhang, and Xin Yang. Wricnet: A weighted rich-scale inception coder network for remote sensing image change detection. *IEEE Transactions on Geoscience and Remote Sensing*, 60:1–13, 2022. [1, 2](#)
- [22] Tommie Kerssies, Niccolò Cavagnero, Alexander Hermans, Narges Norouzi, Giuseppe Averta, Bastian Leibe, Gijs Dubbelman, and Daan de Geus. Your vit is secretly an image segmentation model. In *Proceedings of the Computer Vision and Pattern Recognition Conference*, pages 25303–25313, 2025. [2](#)
- [23] MA Lebedev, Yu V Vizilter, OV Vygolov, Vladimir A Knyaz, and A Yu Rubis. Change detection in remote sensing images using conditional adversarial networks. *The International Archives of the Photogrammetry, Remote Sensing and Spatial Information Sciences*, 42:565–571, 2018. [5](#)
- [24] Tao Lei, Xinze Geng, Hailong Ning, Zhiyong Lv, Maoguo Gong, Yaochu Jin, and Asoke K Nandi. Ultralightweight spatial-spectral feature cooperation network for change detection in remote sensing images. *IEEE Transactions on Geoscience and Remote Sensing*, 61:1–14, 2023. [2](#)
- [25] Miao Li, Dongping Ming, Lu Xu, Dehui Dong, and Yu Zhang. Sfearnet: A network combining semantic flow and

edge-aware refinement for highly efficient remote sensing image change detection. *IEEE Transactions on Geoscience and Remote Sensing*, 2025. 6, 7

[26] Qingyang Li, Ruofei Zhong, Xin Du, and Yu Du. Tran-sunetc: A hybrid transformer network for change detection in optical remote-sensing images. *IEEE Transactions on Geoscience and Remote Sensing*, 60:1–19, 2022. 2, 3

[27] Zhenglai Li, Chang Tang, Xinwang Liu, Wei Zhang, Jie Dou, Lizhe Wang, and Albert Y Zomaya. Lightweight remote sensing change detection with progressive feature aggregation and supervised attention. *IEEE Transactions on Geoscience and Remote Sensing*, 61:1–12, 2023. 2

[28] Mengxi Liu, Zhuoqun Chai, Haojun Deng, and Rong Liu. A cnn-transformer network with multiscale context aggregation for fine-grained cropland change detection. *IEEE Journal of Selected Topics in Applied Earth Observations and Remote Sensing*, 15:4297–4306, 2022. 3

[29] Wenyu Liu, Jindong Li, Haoji Wang, Run Tan, Yali Fu, and Qichuan Tian. Lcd-net: A lightweight remote sensing change detection network combining feature fusion and gating mechanism. *IEEE Journal of Selected Topics in Applied Earth Observations and Remote Sensing*, 2025. 7

[30] Yi Liu, Chao Pang, Zongqian Zhan, Xiaomeng Zhang, and Xue Yang. Building change detection for remote sensing images using a dual-task constrained deep siamese convolutional network model. *IEEE Geoscience and Remote Sensing Letters*, 18(5):811–815, 2020. 2

[31] Ze Liu, Yutong Lin, Yue Cao, Han Hu, Yixuan Wei, Zheng Zhang, Stephen Lin, and Baining Guo. Swin transformer: Hierarchical vision transformer using shifted windows. In *Proceedings of the IEEE/CVF international conference on computer vision*, pages 10012–10022, 2021. 3

[32] Zhiyong Lv, Fengjun Wang, Guoqing Cui, Jón Atlí Benediktsson, Tao Lei, and Weiwei Sun. Spatial–spectral attention network guided with change magnitude image for land cover change detection using remote sensing images. *IEEE Transactions on Geoscience and Remote Sensing*, 60:1–12, 2022. 2

[33] Jingjing Ma, Junyi Duan, Xu Tang, Xiangrong Zhang, and Licheng Jiao. Eatder: Edge-assisted adaptive transformer detector for remote sensing change detection. *IEEE Transactions on Geoscience and Remote Sensing*, 62:1–15, 2024. 6, 7

[34] Mubashir Noman, Mustansar Fiaz, Hisham Cholakkal, Salman Khan, and Fahad Shahbaz Khan. Elgc-net: Efficient local–global context aggregation for remote sensing change detection. *IEEE Transactions on Geoscience and Remote Sensing*, 62:1–11, 2024. 2, 3, 5, 6, 7, 8

[35] Mubashir Noman, Mustansar Fiaz, Hisham Cholakkal, Sanath Narayan, Rao Muhammad Anwer, Salman Khan, and Fahad Shahbaz Khan. Remote sensing change detection with transformers trained from scratch. *IEEE Transactions on Geoscience and Remote Sensing*, 62:1–14, 2024. 2, 3, 7

[36] Daifeng Peng, Yongjun Zhang, and Haiyan Guan. End-to-end change detection for high resolution satellite images using improved unet++. *Remote Sensing*, 11(11):1382, 2019. 1, 2

[37] Qian Shi, Mengxi Liu, Shengchen Li, Xiaoping Liu, Fei Wang, and Liangpei Zhang. A deeply supervised attention metric-based network and an open aerial image dataset for remote sensing change detection. *IEEE transactions on geoscience and remote sensing*, 60:1–16, 2021. 5

[38] Michele Volpi, Devis Tuia, Francesca Bovolo, Mikhail Kanevski, and Lorenzo Bruzzone. Supervised change detection in vhr images using contextual information and support vector machines. *International Journal of Applied Earth Observation and Geoinformation*, 20:77–85, 2013. 1

[39] Bin Wang, Xiaohu Jiang, Pinle Qin, and Jianchao Zeng. Dsfcd: Joint distribution sampling and feature decoupling deep network for remote sensing change detection. *IEEE Transactions on Geoscience and Remote Sensing*, 2025. 6, 7

[40] Liangjun Wang, Weitao Chen, Haoyi Wang, and Zhengchao Chen. A novel transformer-based multiscale siamese framework for high-resolution remote sensing change detection. *IEEE Journal of Selected Topics in Applied Earth Observations and Remote Sensing*, 2025. 6, 7

[41] Enze Xie, Wenhui Wang, Zhiding Yu, Anima Anandkumar, Jose M Alvarez, and Ping Luo. Segformer: Simple and efficient design for semantic segmentation with transformers. *Advances in neural information processing systems*, 34:12077–12090, 2021. 6, 8

[42] Zhongxiang Xie, Shuangxi Miao, Yuhang Jiang, Zhewei Zhang, Jing Yao, Xuecao Li, Jianxi Huang, and Pedram Ghamisi. Fsg-net: Frequency-spatial synergistic gated network for high-resolution remote sensing change detection. *arXiv preprint arXiv:2509.06482*, 2025. 2, 6, 7

[43] Chenhongyi Yang, Zehui Chen, Miguel Espinosa, Linus Ericsson, Zhenyu Wang, Jiaming Liu, and Elliot J Crowley. Plainmamba: Improving non-hierarchical mamba in visual recognition. *arXiv preprint arXiv:2403.17695*, 2024. 3

[44] Feng Yang, Mengtao Li, Wenqiang Shu, Anyong Qin, Tiecheng Song, Chenqiang Gao, and Gui-Song Xia. Conformer-ed: Hybrid cnn-transformer with temporal attention for detecting changes in remote sensing imagery. *IEEE Transactions on Geoscience and Remote Sensing*, 2025. 6, 7

[45] Jianwei Yang, Chunyuan Li, Xiyang Dai, and Jianfeng Gao. Focal modulation networks. *Advances in Neural Information Processing Systems*, 35:4203–4217, 2022. 5, 7, 8

[46] Yijun Yang, Zhaohu Xing, Lequan Yu, Chunwang Huang, Huazhu Fu, and Lei Zhu. Vivim: A video vision mamba for medical video segmentation. *arXiv preprint arXiv:2401.14168*, 2024. 3

[47] Chenxiao Zhang, Peng Yue, Deodato Tapete, Liangcun Jiang, Boyi Shangguan, Li Huang, and Guangchao Liu. A deeply supervised image fusion network for change detection in high resolution bi-temporal remote sensing images. *ISPRS Journal of Photogrammetry and Remote Sensing*, 166:183–200, 2020. 2

[48] Cui Zhang, Liejun Wang, Shuli Cheng, and Yongming Li. Swinsunet: Pure transformer network for remote sensing image change detection. *IEEE Transactions on Geoscience and Remote Sensing*, 60:1–13, 2022. 3

[49] Hongyan Zhang, Manhui Lin, Guangyi Yang, and Liangpei Zhang. Escnet: An end-to-end superpixel-enhanced change

detection network for very-high-resolution remote sensing images. *IEEE Transactions on Neural Networks and Learning Systems*, 34(1):28–42, 2021. 2

[50] Haotian Zhang, Hao Chen, Chenyao Zhou, Keyan Chen, Chenyang Liu, Zhengxia Zou, and Zhenwei Shi. Bifa: Remote sensing image change detection with bitemporal feature alignment. *IEEE Transactions on Geoscience and Remote Sensing*, 62:1–17, 2024. 3

[51] Haotian Zhang, Keyan Chen, Chenyang Liu, Hao Chen, Zhengxia Zou, and Zhenwei Shi. Cdmamba: Incorporating local clues into mamba for remote sensing image binary change detection. *IEEE Transactions on Geoscience and Remote Sensing*, 2025. 3, 6, 7

[52] Hong Zhang, Yuhang Teng, Haojie Li, and Zhihui Wang. Strobustnet: Efficient change detection via spatial-temporal robust representations in remote sensing. *IEEE Transactions on Geoscience and Remote Sensing*, 2025. 3, 6, 7

[53] Min Zhang and Wenzhong Shi. A feature difference convolutional neural network-based change detection method. *IEEE Transactions on Geoscience and Remote Sensing*, 58(10):7232–7246, 2020. 2

[54] Sijie Zhao, Hao Chen, Xueliang Zhang, Pengfeng Xiao, Lei Bai, and Wanli Ouyang. Rs-mamba for large remote sensing image dense prediction. *IEEE Transactions on Geoscience and Remote Sensing*, 2024. 2, 3, 6, 7

[55] Lianghui Zhu, Bencheng Liao, Qian Zhang, Xinlong Wang, Wenyu Liu, and Xinggang Wang. Vision mamba: Efficient visual representation learning with bidirectional state space model. *arXiv preprint arXiv:2401.09417*, 2024. 3